

1 **Characterisation and pore structure analysis of mortar incorporating valorised rice husk**
2 **ash**

3
4 Author 1

- 5 • Arshdeep Singh, Assistant Professor
6 • Department of Civil Engineering, Punjab Engineering College, Chandigarh,160012,India

7 Author 2

- 8 • Bhupinder Singh, Ph.D.
9 • Department of Civil Engineering, Indian Institute of Technology Roorkee, Roorkee,
10 Uttarakhand, 247667, India

11 Author 3

- 12 • P.S. Mangat, Ph.D.
13 • Centre for Infrastructure Management, Materials and Engineering Research Institute,
14 Sheffield Hallam University, Sheffield S1 1WB, UK

15
16 **Full contact details of corresponding author.**

17
18 Arshdeep Singh,

19 Assistant Professor,

20 Department of Civil Engineering,

21 Punjab Engineering College, Chandigarh,160012, India.

22 E-mail: *singharsh004@gmail.com*

23

24

25

26

27

28

29

30

31

32

33

34

35

36 **Abstract**

37 Physical, chemical, and mineralogical characterisation of as-received Rice Husk Ash (RHA)
38 samples sourced from four rice-growing regions (North, South, East, and West) of India is
39 presented. Valorised RHA was obtained through controlled combustion at two temperature
40 ranges (600°C–700°C and 650°C–700°C) of husks from the North in an industry set up.
41 Valorisation efficacy has been tested through comparative characterisation of the valorised
42 RHAs with the as-received RHAs from the four regions. Blending of 15% valorised RHA (in the
43 beneficiated state) by weight of cement had no adverse effect on compressive strength even
44 though water-binder ratio of the blended mortar had to be increased by 14% to achieve flow of
45 the control cement mortar. Compared to the control cement mortar, porosity of the mortar
46 blended with the beneficiated RHA measured using Mercury Intrusion Porosimetry increased by
47 up to 10% primarily due to an increase in the number of large mesopores (0.01-0.05 µm).

48

49 Keywords: Rice husk ash, Pozzolans, Reactivity, Supplementary Cementitious Material,
50 Compressive strength.

51

52

53

54

55

56

57

58

59

60

61

62

63 **1. Introduction**

64 Estimated annual production of paddy in India is about 169 Million Tonnes (MT) (FAO RMM
65 2018) and its processing generates approximately one-fifth the weight of paddy as rice husks
66 (Dizaji et al. 2019). It is also estimated that about one-fifth of the weight of these husks is
67 converted into Rice Husk Ash (RHA) when for example rice husk is used as a fuel in energy co-
68 generation processes (Singh 2018). Currently, most of this ash in the country is disposed off in
69 landfills or simply dumped in the open. Due to combustion variabilities inherent in industries
70 consuming rice husks as a fuel, significant scatter in the physical, chemical, and mineralogical
71 properties of RHAs is reported in the literature (Dizaji et al. 2019; Zunino and Lopez 2017; Rêgo
72 et al. 2015). In the context of combustion conditions, two studies report that residual carbon in
73 RHA obtained from five to ten different industrial sources has been found to vary in the ranges
74 2%-24% (Zunino and Lopez 2017) and 2%-15% (Rêgo et al. 2015a). Since rice husk
75 combustion conditions are reported to have the most significant influence on RHA properties,
76 some of the optimum combustion temperature ranges reported in the literature based on small-
77 scale pilot tests are 660°C – 720°C (Chen et al. 2015); 750°C – 850°C (Nehdi et al. 2003);
78 700°C – 900°C (Blissett et al. 2017) and 700°C (Fernandes et al. 2016). Recommendations
79 have also been made for airflow rates that result in the most optimum ash properties (Chen et
80 al. 2015; Rozainee et al. 2008; Armesto et al. 2002). In addition, ash characteristics are also
81 reported to be influenced by combustion technology (Fernandes et al. 2016; Zain et al. 2011),
82 rate of heating (Chandrasekhar et al. 2006), and dwell time (Nair et al. 2006). For example, the
83 optimum combustion temperature range for an expanded bed reactor is reported to be 700°C –
84 900°C (Blissett et al. 2017) whereas this range for a fluidised bed reactor is 660°C – 720°C
85 (Chen et al. 2015). Considering the large number of parameters that can affect ash
86 characteristics, significant variations in the quality of ash across different geographies of a vast
87 country like India can be expected. This in turn can pose a challenge for the development of
88 over-arching performance specifications for use of RHA as a supplementary cementitious
89 material. The first step towards addressing this problem is characterization of ash from the
90 representative geographies with the second step being investigation of ash valorisation options
91 followed by testing the performance of ash as a Supplementary Cementitious Material (SCM).
92 The target properties in a valorisation strategy can be taken from IS 269: 2015 (BIS 2015) which

93 inter alia requires an amorphous silica content of more than 80% and a residual carbon content
94 < 5% for an acceptable SCM.

95 In this investigation, RHA samples of unknown combustion histories were collected from the
96 North, East, South, and West regions of India respectively. Characterisation of these as-
97 received ashes indicated the need for heat treatment since all of them had unburnt carbon
98 >13%. In the literature, re-burning of ashes to remove excess unburnt carbon had been
99 reported as a valorisation option (Ganesan et al. 2008; Mali and Nanthagopalan 2021), though
100 this option will increase ash processing cost. In the valorisation exercise, control ashes of this
101 study were produced by combusting at 2 temperature ranges locally available husks in the
102 atmospheric fluidised bed boiler of an industrial partner, Kuantum Papers, located in the state of
103 Punjab, India. Comparative characterisation of the four RHAs of unknown combustion history
104 and the two control RHAs is reported together with those of three beneficiated ashes obtained
105 through grinding (for varying intervals of time) of the 2 control ashes.

106 Some studies in the literature (Xu et al. 2012; Van et al. 2013) on RHA blended mortars
107 and concretes report the use of RHA with an average particle size in the range of 0.15 μm -
108 10 μm . It is reckoned that this size range will require fine grinding of ash which may add to its
109 processing cost. As an alternate and more practical option, in this investigation the role of
110 beneficiated RHA as a SCM has been examined for a more realistic level of fineness defined as
111 at least 66% of the sample passing through a 45 μm sieve. This requirement corresponds to the
112 minimum acceptable fineness limit for a Class N raw or calcined natural pozzolana in the ASTM
113 C 618 (ASTM 2019). Notably, the relevant Indian Code, IS 269 (BIS 2015) has no
114 recommendations for the minimum fineness of RHA proposed to be used as SCM.

115 In the limited studies in the literature (Gastaldini et al. 2009; Huang et al. 2017) pore size
116 distribution in RHA blended mixtures has been reported in the form of comparison with plain
117 cement mortar and concrete mixtures having the same water-binder ratios. It implies that super-
118 plasticisers were used in the RHA blended mixtures for obtaining comparable flow behaviour.
119 Chindaprasirt et al. 2007 noted that mortar blended with 20% RHA and containing extra water
120 showed better compressive strength relative to the control mortar made with OPC as the only
121 binder. No superplasticiser was used in this study to compensate for the potential loss of
122 workability due to RHA since authors' attention was to investigate the effect of additional water

123 (up to maximum limit of 115% of control as per ASTM C 618) on the pore structure properties of
124 valorised RHA blended mortars. Recommendations are made for optimum rice husk
125 combustion conditions and desirable RHA physical, chemical and mineralogical characteristics.
126 Guidelines are also given for optimum weight replacement of cement with RHA in blended
127 mortars.

128 **2. Materials and methods**

129 **2.1 Materials**

130 Summary of the four as-received RHA samples of unknown combustion histories (R1, R2,
131 R3, R4), two control RHAs (R5 and R6), and the beneficiated RHAs is presented in **Table S1**.
132 Beneficiation of the control RHAs was carried out by grinding using a Los Angeles machine with
133 a material-to-charge ratio of 1:3. The R5 sample was ground for 60 min, and 100 min. Based on
134 the consistency and compressive strength results of the beneficiated R5 sample, the R6 sample
135 was only ground for 100 minutes. In **Table S1**, the beneficiated R5 samples are identified as
136 'R5-G60', and 'R5-G100' and the R6 sample is identified as 'R6-G100'. Ordinary Portland
137 Cement (OPC) of 43 Grade, having a specific gravity of 3.15 and conforming with IS 269 (BIS
138 2015) having Loss-On-Ignition (LOI) 2.19%, and standard sand conforming with IS 650 (BIS
139 1991) was used in the pastes and mortars which were tested as per relevant Indian standards.

140 **2.2 RHA characterization**

141 **2.2.1 Chemical characterisation**

142 Chemical composition of the RHA samples was evaluated using X-Ray Fluorescence
143 (XRF) and is reported in **Table 1**. Loss-On-Ignition (LOI) test was performed in accordance with
144 IS 1727 (BIS, 1967) to check the percentage of unburnt carbon.

145 **2.2.2 Mineralogical characterisation**

146 Mineralogical characterisation was carried out using X-Ray Diffraction (XRD). The RHA
147 samples were analysed using Cu K α radiation ($\lambda=1.5402\text{\AA}$) and Co K α radiation ($\lambda=1.789\text{\AA}$) at
148 an angle (2θ) range of 5° to 100° using a scanning rate of $0.013^\circ/\text{s}$. An internal standard method
149 was used to estimate total amorphous content in the RHA samples.

150 **2.2.3 Physical characterisation**

151 Physical characteristics in terms of fineness, specific gravity, surface area, and morphology
152 were investigated in the as-received as well as in the other samples. Morphological studies
153 were carried out using a scanning electron microscope. Brunauer–Emmett–Teller specific
154 surface area (BET-SSA) was measured using a multi-point BET test and values were rounded
155 off to the nearest ± 0.5 . The average particle size of the RHAs was examined using laser particle
156 diffraction.

157 **2.2.4 Pozzolanic reactivity**

158 A volume replacement of cement with 20% RHA was done to measure the pozzolanic reactivity
159 of RHA as per IS 1727 (BIS 1967). This test was performed on cement mortars. The percentage
160 compressive strength of the blended cement mortar 50 mm size cubes with respect to the
161 reference specimen (with cement as the only binder) was determined after 7 and 28-days of
162 moist curing and used for calculation of pozzolanic reactivity. Samples R1, R2, R3, and R4 were
163 investigated in the as-received state only. Flowability across all mortars was maintained in the
164 range of $105 \pm 5\%$.

165 **2.3 Standard consistency**

166 Standard consistency of the RHA blended cement pastes was determined in accordance with IS
167 4031 (Part 4) (BIS 1988) for 5%, 10%, 15%, and 20% weight replacements of cement with the
168 selected RHA. This test was carried out on the R5 sample (control and beneficiated) only. The
169 quantity of water taken for each cube was $(P/4+3)$ percent of the combined mass of binder and
170 sand as recommended in IS 4031 (Part 6) (BIS 1988), where P is the percentage of water
171 required to produce a paste of standard consistency.

172 **2.4 Compressive strength**

173 Amongst the control ashes, the R5 sample was tested as per relevant Indian standards and the
174 R6 sample was tested as per ASTM standards. Compressive strengths of mortars blended with
175 the R5 sample were investigated using 70.6 mm cubes in accordance with IS 4031 (Part 6) (BIS
176 1988). For each cube, 200 g of binder was mixed with 600 g of standard sand. The R5 sample

177 was tested in both the beneficiated and the unbeneficiated states and weight replacements of
178 cement with RHA were 5%,10%,15%, and 20%.

179 Compressive strengths of the Plain Cement (PC) mortars (serving as the reference
180 material) and the mortars blended with the beneficiated R6 sample (R6-G100) was tested in
181 accordance with ASTM C 109 (ASTM 2020) for 10%,15%, and 20% weight replacements of
182 cement with RHA. The binder-sand ratio was 1:2.75 and for each of the RHA replacement
183 levels and water-binder ratio that produced $110 \pm 5\%$ flow of mortar was used. The mortar
184 specimens were demoulded after 24 hrs and moist cured at $27 \pm 2^\circ\text{C}$ until the test ages of 7-
185 and 28-days. All the reported compressive strength results are the averages of three replicate
186 samples. Qualitative microstructure analysis of the PC mortar and RHA (R6-G100) blended
187 mortars was also performed using XRD, scanning electron microscopy (SEM) and Energy
188 Dispersive X-Ray Analysis (EDX).

189 **2.5 Mercury intrusion porosimetry**

190 To investigate pore size distribution and total porosity, Mercury Intrusion Porosimetry (MIP)
191 was performed on the PC and the mortars blended with the beneficiated RHA (R6-G100). The
192 test samples were obtained from the mortar cubes cast for 28-day compressive strength testing.
193 At least three pieces each approximately 6-8 mm square and 0.7-1g in weight were taken from
194 the inner core of the cube specimens. First, these samples were placed inside an oven
195 ($100 \pm 5^\circ\text{C}$) for 3 days to completely remove pore water and then placed inside a desiccator for 3
196 days. After this conditioning the samples were stored in a sealed plastic bag till testing. MIP was
197 carried out on both blended and unblended mortars using a Pascal 140/240 Porosimeter which
198 measures pore sizes in the range of 0.0073 to $100\mu\text{m}$. The Washburn Equation, **(Eq. (1))** was
199 used to relate applied pressure to pore diameter.

$$200 \quad p = \frac{2\gamma \cos \phi}{r} \quad (1)$$

201 where p is absolute applied pressure, r is pore radius, ϕ is the contact angle ($=140^\circ$), γ is
202 mercury surface tension ($= 0.48 \text{ N/m}$).

203 3. Results and Discussion

204 3.1 RHA characterization

205 3.1.1 Chemical characterisation

206 As per **Table 1**, silicon dioxide (SiO_2) in R1, R2 & R4 is 61.3%, 70%, and 72.2%
207 respectively. Only R3, R5, and R6 have SiO_2 contents that are equal to or more than 80%. The
208 high LOI in R1 and R2 is associated with reduced silica content in these samples and the low
209 silica content in R4 is attributed to both its high potassium oxide (K_2O) content and high residual
210 carbon. In terms of percentage of SiO_2 , the characteristics of the studied control RHA samples
211 were found to be similar with the properties of RHAs of other Asian countries reported by (Zain
212 et al. 2011; Xu et al. 2012; and Venkatanarayanan and Rangaraju 2013). However as observed
213 in the studied RHA samples, a linear decreasing trend of SiO_2 content in RHA with increase in
214 unburnt carbon was also reported by (Venkatanarayanan and Rangaraju 2013). SiO_2 content in
215 RHA may also reduce in the presence of high K_2O (Bie et al. 2018). **Table 1** shows the
216 chemical requirements of RHA samples which were compared with chemical requirements of
217 ASTM C 618 (ASTM 2019) for Class N-raw or calcined natural pozzolanas, BS 8615-2 (BSI
218 2019) for high reactivity natural calcined pozzolana, and IS 269 (BIS 2015) for RHA. The 80%
219 amorphous silica requirement of IS: 269 (BIS 2015) was not fulfilled by any of the RHA samples
220 except for R6. However, the requirement of 70% combined oxides of silica, alumina, and ferrite
221 (SAF) of ASTM C 618 (ASTM 2019) and BS 8615-2 (BSI 2019) was satisfied by all the RHAs
222 except for R1. **Table 1** shows that none of the RHAs had unburnt carbon content below the 5%
223 upper-bound limit of IS: 269 (BIS 2015) although for the control ashes (R5 and R6), LOI was
224 within the upper-bound limit (10%) for Class N-raw or calcined natural pozzolans of ASTM C
225 618 (ASTM 2019). As per BS 8615-2 (BSI 2019) upper limit for unburnt carbon in natural
226 calcined pozzolana is 7%.

227 3.1.2 Mineralogical Characterisation

228 **Figure S1(a)** presents the X-ray diffractograms (XRD) of R1, R2, R3, R4, R5, and R6.
229 The R1 and R2 samples were found to be purely amorphous since no crystalline peak was
230 noticed in their XRDs. Since residual carbon is also amorphous in nature, it may be responsible

231 for the high total amorphous content in these ashes (Batra et al. 2008). The presence of peaks
232 in the R3 and R4 samples is indicative of the partially crystalline nature of these ashes. For a
233 more objective analysis, the amorphous fraction in each sample was also evaluated using an
234 internal standard method in which a precisely known quantity of an internal standard (i.e. pure
235 silicon) was added to each RHA sample before XRD analysis followed by the Rietveld
236 refinement of XRDs. As an illustration of such an analysis, XRDs of R5, and R6 obtained after
237 the addition of standard silicon are presented in **Figures S1(b)** and **S1(c)** respectively. Analysis
238 of these diffractograms indicates that in all the RHA samples the primary crystalline phases
239 were cristobalite and quartz. In the R4, R5, and R6 samples, the total amorphous fraction
240 (inclusive of all oxides) was more than 90% whereas the percentage of amorphous silica was
241 64%, 70%, and 80% respectively, **Table 1**. It may be noted that as per IS: 269 (BIS 2015) the
242 minimum acceptable amorphous silica content in RHA is 80%. Another study, (Olalekan and
243 Mangat 2018) reports reactive silica content of 70% -72% in Indian RHAs. (Zunino and Lopez
244 2017) concluded that RHA can be considered a promising pozzolanic material despite having
245 substantial variation in the amorphous silica content which was 38% to 85%. As per BS 8615-2
246 (BSI 2019), amorphous silica in natural calcined pozzolanas should be more than 25% whereas
247 no such limit is set by ASTM C 618 (ASTM, 2019). However, finely ground RHA having 17.66 %
248 amorphous silica also showed adequate pozzolanic reactivity as studied by (Rêgo et al. 2015a).
249 Hence, in the context of the BSI and ASTM requirements, R5 and R6 qualify as pozzolanic
250 materials and the IS Code requirements seem to be overly restrictive.

251 Keeping this in mind, the authors are of the opinion that the replacement percentage of
252 RHA should be decided in such a way that the total unburnt carbon of the binary binder
253 (OPC+RHA) does not exceed the Indian Standard IS 269 (BIS 2015) specified maximum
254 unburnt carbon limit of 5% for OPC. In this investigation, LOI of the cement and RHA (R6) was
255 2.19% and 7.3% respectively, and the maximum unburnt carbon in the binary blend of 80%
256 OPC+20% control RHA (R6) was 3.21%.

257 **3.1.3 Physical characterisation**

258 **3.1.3.1 Fineness**

259 Measured physical properties are presented in **Table 1**. The wet sieve analysis results
260 show that more than 80% of all the material in the as-received and in the control ashes was
261 coarser than 45 μm which is neither in compliance with the fineness requirement for Class N-
262 raw or calcined natural pozzolans in ASTM and BSI nor with any of the Indian Codes for
263 pozzolanic materials. For example, IS 3812 (Part 1) (BIS 2013) specifies that in the case of fly
264 ash not more than 34% of the particles should be retained on a 45 μm sieve. The specific
265 gravity of the RHAs was found to be higher in the control ashes when compared to the as-
266 received ashes. High LOI has been reported to decrease the specific gravity in sugar-cane
267 bagasse ash (Mali and Nanthagopalan 2021) and the results in **Table 1** lend support to this
268 finding. **Table 1** shows that RHA beneficiated through grinding for 60 minutes at a material-to-
269 charge ratio of 1:3 satisfied the ASTM C 618 (ASTM 2019) and the BS 8615-2 (BSI 2019)
270 minimum fineness requirement of at least 66% and 60% passing from 45 μm respectively. It
271 may be noted that the average particle size of the R5 sample decreased significantly from 171
272 μm in its unbeneficiated state to 22 μm and 18 μm for grinding durations of 60 min and 100 min
273 respectively. In the case of the R6 sample, average particle size in its beneficiated state was 25
274 μm compared to 228 μm in the unbeneficiated state. Similar level of fineness was obtained by
275 (Rego et al. 2015b) using LOS Angeles test arrangement for 60 min grinding.

276 **3.1.3.2 BET Specific Surface Area**

277 BET Specific Surface Area (BET-SSA) of the RHAs varied in the wide range of 15 m^2/g
278 - 50 m^2/g , **Table 1**. The higher BET-SSA in the ashes from the East (R1) and South (R2) is
279 attributed to their higher unburnt carbon content. Since a high K_2O content is reported to
280 decrease surface area (Bie et al. 2018), the lower surface area in R4 is attributed to its high K_2O
281 content. Effect of grinding on BET-SSA of the control ashes (R5 and R6) may be seen with
282 reference to **Table 1**. In the unbeneficiated control RHA samples R5 and R6, BET-SSA was 26
283 m^2/g and 32 m^2/g which increased to 35 m^2/g and 43 m^2/g respectively after beneficiation.

284 **3.1.3.3 Morphology**

285 Cellular microstructure was seen in the morphology of all the as-received ash samples,
286 **Figure 1**, with pores being seen on the particle surface in some cases, **Figures 1 (b)** and **1 (d)**.
287 Morphology of the beneficiated ashes is shown in **Figures 1 (g)** and **1 (h)** where agglomeration

288 of very fine particles with the coarser ones can be seen. Similar behaviour is also reported by
289 (Rego et al. 2015b). Most of the macropores present on the surface of the as-received RHAs
290 collapsed after grinding. As highlighted in **Figures 1 (g)** and **1 (h)**, surface pores continue to be
291 present in the beneficiated ashes in spite of grinding. These fine pores on the surface are
292 responsible for the large surface area which in turn imparts high pozzolanic reactivity.

293 **3.1.4 Pozzolanic reactivity**

294 According to IS 269 (BIS 2015), pozzolanic reactivity of RHA when examined in
295 accordance with IS 1727 (BIS 1967), should be more than 90%. The 7-day and 28-day
296 compressive strength results in **Table 1** show that none of the as-received RHA samples and
297 the control RHA samples fulfilled this requirement. However, all the beneficiated RHA samples
298 achieved strengths of more than 90% of the strength of the reference specimen. The increase in
299 water demand due to the inclusion of R1 and R2 in binary binders was more than the maximum
300 permissible limit of 115% of control in ASTM C 618 (ASTM 2019), **Table 1**. Binary binders
301 including the beneficiated RHAs showed the least increase in water demand which was in the
302 range of 105% - 110% of the reference. The low 28-day pozzolanic reactivity of R1 and R2 is
303 attributed to their higher LOI (33% and 23.4% respectively) which leads to an increase in water
304 demand for achieving the same flow as the reference sample. In **Table 1**, the high strength
305 obtained with the beneficiated RHAs is attributed to the lower water-binder ratio and better
306 reactivity due to the presence of fine particles as well as to the filler effect of such particles.

307 **3.2 Standard consistency**

308 Typical trends in standard consistency are presented in **Figure 2 (a)** which shows that
309 the consistency of paste blended with the R5 control ash varied from 121% of that for the
310 reference paste at 5% replacement level to 171% for 20% replacement. However, in the case of
311 the beneficiated samples, at 5% replacement levels, consistency varied from 111% of the
312 reference paste to 139% for 20% RHA replacement. Standard consistency of the unblended
313 cement paste (taken as reference) was 28%. To illustrate the effect of beneficiation, the
314 consistency of pastes blended with R5, R5-G60, and R5-G100 at 15% replacement level was
315 154%, 129%, and 132% of the reference paste respectively. This indicates that more water is
316 required to maintain paste consistency with the control RHA R5 when compared to its

317 benefited counterparts R5-G60 and R5-G100. This behaviour is attributed to a breakdown in
318 the pore structure of the RHA particles in the benefited samples. **Figure 2 (b)** shows that the
319 mortar water-binder ratio calculated using the consistency of the relevant paste is higher at
320 each replacement level of the control RHA, R5. Further, this figure also shows that at each of
321 the replacement levels (5%, 10%, 15%, and 20%) mortars blended with the benefited R5 has
322 relatively lower water demand when compared to mortars containing the unbeneficiated ash. It
323 may be seen in **Figure 2 (b)** that increased water demand for R5 was within the allowable limit
324 of 115% in ASTM C 618 (ASTM 2019) only as long as the cement replacement level was
325 capped at 5% and for the benefited R5 this limit was 10%.

326 **3.3 Compressive strength**

327 Strength testing was done only with the control and the benefited ashes. Results of sample
328 R5 are discussed here which are typical of the RHAs under investigation. **Figures 3 (a) and 3**
329 **(b)** respectively present 7- and 28-day compressive strength of the reference cement mortar
330 vis-à-vis the RHA (R5) blended cement mortar for up to 20% RHA replacement levels. These
331 figures show that across all the RHA replacement levels, higher strengths were obtained with
332 the benefited ash when compared to the control R5. Further, a decreasing trend in
333 compressive strength of benefited RHA blended mortars is observed with increasing
334 replacement levels. Compressive strength exceeding 80% of the strength of the reference
335 mortar (with only cement as the binder) was achieved for up to 15% replacement of cement with
336 R5-G100 at both test ages. In comparison, the compressive strength of the control RHA R5 is
337 less than 50% of the reference mortar at 15% replacement of RHA as shown in **Figures 3 (a)**
338 **and 3 (b)**. **Figure 3 (c)** shows the compressive strength variation in the PC and the RHA (R6-
339 G100) blended mortars investigated as per ASTM C 109 (ASTM 2020) for $110 \pm 5\%$ flow. It may
340 be observed in this figure that to obtain flow similar to that of the PC mortar, the water-to-binder
341 ratio increased linearly for up to 15% replacement level following which it remained constant up
342 to 20% replacement level of RHA. A 28-day compressive strength of 95% and 92% of that of
343 the PC mortar was achieved up to a replacement level of 15% and 20% respectively. The
344 increase in water-binder ratio was up to 14% of that of the PC mortars prepared for $110 \pm 5\%$
345 flow with no significant reduction in compressive strength. This observation is similar to that
346 made by (Chindaprasirt et al. 2007) wherein it was noted that mortar blended with 20% RHA

347 and containing extra water showed better compressive strength relative to the control mortar
348 made with OPC as the only binder. The XRD analysis of mortars show the reduction in
349 portlandite which is a crystalline phase of calcium hydroxide as shown in **Figure S2** and lower
350 Ca/Si ratios of RHA blended mortars reported in SEM and EDS results in **Figure S3** are
351 indicative of pozzolanic reaction of cement with RHA. Morphological properties of hydration
352 products of lower Ca/Si ratio are supportive in the pore refinement of mortars (Rego et al.
353 2015a) which is in compliance with the results of mercury intrusion porosimetry tests reported
354 on mortars in Section 3.4.

355 Hence, the compressive strength results obtained in the context of both the Indian and
356 the ASTM standards indicate that the beneficiated RHA up to 15% weight replacement of
357 cement can be used in cement mortar without any detrimental effect on 7- and 28-day
358 compressive strength, as long as the fineness of the ash complies with the minimum
359 requirement of ASTM C 618-19 or BS 8615-2 (BSI 2019) and amorphous silica content
360 requirement in the IS 269: 2015 is relaxed from 80% so that in the context of this Code the
361 beneficiated ashes also become acceptable as a pozzolan. Thus, combining the guidelines of
362 Indian, British and ASTM Standards, RHA can be recommended for use in concrete if at least
363 60% particles are finer than 45 μm , SAF is > 70%, amorphous silica content is >25% and LOI of
364 binary binder (OPC+RHA) is below 5%.

365 **3.4 Mercury intrusion porosimetry**

366 **3.4.1 Pore Size Distribution**

367 The relationship between pore diameter, differential pore volume, and cumulative pore
368 volume for the plain cement mortar and the beneficiated RHA blended mortars is presented in
369 **Figures S4 (a), (b), (c) and (d)** respectively. Zones with zero differential pore volume are
370 termed as non-porous and zones showing significant differential pore volume are called porous.
371 Both non-porous and porous zones were present in the measured range of pore diameters.
372 Similar to results in the literature (Mangat and Ojedokun 2018), the beneficiated RHA blended
373 mortars showed unimodal pore distribution similar to that observed in the cement mortars and
374 peak pore volume was within the range of 0.01-0.1 μm . As shown in **Figures S4 and 4 (a)**, pore
375 volume distribution in the RHA blended mortars tended to shift towards the lower range of pore

376 sizes. This behaviour is attributed to the dense microstructure achieved in the RHA mortars due
377 to pozzolanic reactions (Wada et al. 2000).

378 **3.4.2 Pore system parameters**

379 The pore system parameters are derived from the cumulative and differential pore
380 volume curves. These parameters play a significant role in assessing the microstructure of
381 cementitious mixtures (Aligizaki 2006; Ma 2014). The representative MIP curves as shown in
382 **Figure S4** provide information on the intrudable porosity (Φ_{in}), threshold pore diameter (d_{th}),
383 and critical pore diameter (d_c). The average pore diameter (d_{avg}) and total porosity can be
384 analyzed from the numerical data. The critical pore diameter corresponds to the peak intruded
385 volume and the threshold pore diameter corresponds to the minimum continuous pore size after
386 which there will be a sharp change in the cumulative pore volume curve. Threshold diameter
387 was identified as the intersection of tangents of the slope changing points on the cumulative
388 curve (Ma 2014).

389 **3.4.2.1 Intrudable and total porosity**

390 The volume of intrudable pores in the PC and the beneficiated RHA (R6-G100) blended
391 mortars was determined from the cumulative pore volume curves and representative results are
392 shown in **Figure 4 (a)** and are presented in **Table 2**. The intrudable volume was 75.42 mm³/g
393 for the PC mortar and was found to be more for both 15% and 20% beneficiated RHA (R6-
394 G100) replacement though the increase was not higher than 6% of that of the PC mortar.
395 Similarly, total porosity also increased with the addition of beneficiated RHA (R6-G100) and was
396 in the range of 102% - 110% of that of the PC mortar. The increase in intrudable and total
397 porosity is attributed to the higher water content used to obtain a flow in the beneficiated RHA
398 (R6-G100) blended mortars similar to that of the PC mortar. On the other hand, (Maeda et al.
399 2001) report lower total porosity in RHA blended mixtures prepared using the same water-
400 binder ratio as the control mixture. It may be observed in **Figure 4 (b)** that filled pore volume is
401 concentrated towards the lower range of pore sizes and this parameter increases with an
402 increase in the percentage of beneficiated RHA (R6-G100).

403 Pore size ranges are classified into capillary pores and gel pores (Mindess et al. 2003).
404 Capillary pores are further divided into macropores (10-0.05 μm) and large mesopores (0.05-
405 0.01 μm) and pores with size $< 0.01\mu\text{m}$ are classified as gel pores. **Table 2** presents the
406 percentage of pore volume filled by each of these pore sizes. Pore refinement was also noted in
407 the higher range of particle sizes. For example, in the particle size range of $>0.05 \mu\text{m}$, the total
408 pore volume in the PC mortar was higher when compared to mortar being prepared with 10%,
409 15%, and 20% beneficiated RHA (R6-G100). The experimental data in **Table 2** shows that the
410 higher water demand associated with the use of beneficiated RHA (R6-G100) does not alter the
411 porosity associated with macropores though the porosity associated with large mesopores
412 increases. The lower porosity of macropores is attributed to the pore refinement due to the
413 denser microstructure of beneficiated RHA blended mortars by pozzolanic reaction (Maeda et
414 al., 2001). Permeability in cement mortars is directly linked with the porosity and pore sizes.
415 According to Aligizaki (Aligizaki 2006), the mechanisms for transport processes are quite
416 different in different categories of pores. In the case of gel pores movement of water does not
417 contribute much to the cement paste permeability. In mesopores having sizes between 0.002
418 and 0.05 μm , electrostatic interactions between the pore liquid and the pore walls may hinder
419 the transport processes but these electrostatic effects do not occur in macropores. It is therefore
420 reckoned that despite its higher total porosity the refined pore structure in mortars blended with
421 the beneficiated RHAs is conducive for restricting the ingress of water or other chemicals when
422 compared to the PC mortars.

423 **3.4.2.2 Pore diameters**

424 The durability properties of cementitious mixtures are influenced by critical and
425 threshold pore diameters (Ma 2014; Mangat and Ojedokun 2018). Threshold diameter can be
426 considered as the property controlling water intrusion in mortar (Dhandapani and Santhanam
427 2017) and in all the mortars of this investigation the threshold diameter varies in the range 2-3
428 μm . **Table 2** shows that despite blending with the beneficiated RHA (R6-G100) and the
429 associated high-water demand, no detrimental effect was observed on threshold diameters in
430 the mortars blended with the beneficiated RHAs when compared to the PC mortars. The critical
431 diameter for the mortar sample containing 10% beneficiated RHA was approximately similar to

432 that of the PC mortar however for the sample containing 15% beneficiated RHA this diameter
433 was significantly lower than that of the PC mortar. However, for the sample containing 20%
434 RHA, two critical pore diameters were observed, one being larger and the other being smaller
435 than the critical size associated with the PC sample. It was also noted that the average pore
436 diameter of each of the beneficiated RHA blended mortars was lower than the average pore
437 diameter of the PC mortar. The reduction in both the critical and the average diameters in the
438 beneficiated RHA (R6-G100) blended mortars is attributed to the shifting of pore size
439 distribution towards the smaller range of pores principally due to the pore refinement by
440 pozzolanic action of RHA. Pore refinement of cement pastes blended with RHA was also
441 reported by (Rego et al. 2015a) which showed reduction in pore volume for the pore sizes
442 higher than 0.05 μm .

443 Although total porosity in the beneficiated RHA up to 20% replacement increased as
444 expected due to high-water dosage when compared to the PC mortar, only the large mesopores
445 (0.05-0.01 μm) have shown an increase in pore volume percentage. Reduction in the total pore
446 volume percentage of macropores in the beneficiated RHA blended mortars and high pore
447 volume percentage in the finer range (0.2-0.05 μm) as shown in **Figure 4 (b)** indicates
448 development of a dense microstructure in the blended mortars when compared to the PC
449 mortar.

450

451 **4. Conclusions**

452 The following conclusions are drawn from the reported investigations:

- 453 a) RHA samples of unknown combustion histories and RHAs obtained from controlled
454 combustion of husks possessed similar fineness. At least an 80% fraction of all the
455 RHAs was coarser than 45 μm . All the RHAs had a cellular microstructure and BET-
456 SSA was in the range of 15 m^2/g – 50 m^2/g .
- 457 b) Loss on Ignition (LOI) of the as-received RHAs from the West, North, South, and the
458 East of the country were 13%, 14%, 23%, and 33% respectively compared to 7% -
459 8% for both the control RHAs (R5 and R6). None of the as-received and the control
460 RHAs satisfied the 5% upper bound LOI limit of IS: 269:2015. However, the LOI
461 values of the control RHAs were below the maximum allowable limit of 10% for

462 Class-N raw or calcined natural pozzolanas given in ASTM C 618-19. Silica content
463 in the as-received RHAs was in the range of 60%-80% whereas it was 80% - 85%
464 for the control RHAs.

465 c) The R6 ash obtained from controlled burning in the temperature range of 650°C-
466 700°C satisfied the 80% amorphous silica requirement of IS: 269:2015 though this
467 was not done by the R5 ash produced at the burning temperature range of 600°C-
468 700°C (70% amorphous silica content). However, both the control ashes R5 and R6
469 fulfilled the chemical and mineralogical requirements of ASTM C 618-19 for Class-N
470 raw or calcined natural pozzolanas. In this context, the 80% amorphous silica
471 requirement in IS 269: 2015 appears to be overly restrictive and will hinder ash
472 utilisation as a supplementary cementitious material.

473 d) Beneficiated RHAs obtained by grinding the control ashes satisfied the minimum
474 fineness requirements for Class-N raw or calcined natural pozzolanas given in the
475 ASTM C 618-19 as well as for fly ash given in the IS 3812 (Part 1): 2013. The
476 beneficiated RHAs also complied with the pozzolanic reactivity requirements of both
477 the IS 269:2015 and the ASTM C 311-18, by achieving >90% pozzolanic reactivity.
478 None of the as-received RHAs fulfilled this minimum pozzolanic reactivity
479 requirement.

480 e) Cement pastes blended with the beneficiated RHAs had lower consistency which
481 translates into lower water/binder ratios and higher strength. In order to obtain RHA
482 blended mortar flow similar to that of the control cement mortar, it can be permissible
483 to increase water content in the blended mortar to 115% of the control value. This
484 increase has been seen to have no detrimental effect on the compressive strength of
485 the blended mortar when compared to its control mortar.

486 f) Pore size distribution in the mortars blended with up to 20% replacement with the
487 beneficiated RHAs shifted towards the lower range of pores and the volume of
488 macropores (10-0.05 μm) in the blended mortars is less than in the PC mortar. On
489 the other hand, the volume of large mesopores (0.05-0.01 μm) was higher in the
490 blended mortars with no significant change in the volume of pores of size < 0.01 μm .

491 However, the total porosity in the blended mortars was 102%-110% of the porosity
492 of the PC mortar.

493 g) Threshold pore diameters in the mortars blended with the beneficiated RHA were
494 comparable to those in the PC mortar or lower. Critical pore diameters and average
495 pore diameters in the blended mortars were lower than those in the PC mortar for up
496 to 15% RHA replacement.

497 h) Compressive strength results obtained in the context of both the relevant Indian and
498 ASTM Standards indicate that up to 15% weight replacement of cement with the
499 beneficiated RHAs can be used in cement mortars without any detrimental effect on
500 the 7- and 28-day compressive strength as long as RHA fineness complies with the
501 ASTM C 618-19 requirements and the amorphous silica content in the IS 269: 2015
502 is relaxed from 80% to 70% leading to the beneficiated ashes also becoming
503 acceptable as pozzolans.

504 **Acknowledgments**

505 Authors acknowledge the Department of Biotechnology, New Delhi, India, to provide a research
506 grant under the aegis of DBT-Innovate, U.K. Newton-Bhabha Fund (BT/IN/Innovate-
507 UK/35/BS/2016-17). We are grateful to our research partners M/s Kuantum Papers Ltd.
508 Hoshiarpur, Punjab, India to provide kind support during the performance of experiments.
509 The first author is grateful to the All India Council for Technical Education and Q.I.P. Centre,
510 Indian Institute of Technology Roorkee, Roorkee, and Commonwealth Scholarship Commission,
511 U.K. for providing a scholarship.

513 **Disclosure Statement**

514 No potential conflict of interest.

515 **References**

516
517 Armesto, L., Bahillo, A., Veijonen, K. et al. 2002. Combustion behaviour of rice husk in a
518 bubbling fluidised bed. *Biomass and Bioenergy* 23(3): 171–179, doi: 10.1016/S0961-
519 9534(02)00046-6.
520 Aligizaki, K.K., 2006. *Pore Structure of Cement-Based Materials: Testing, Interpretation and*
521 *Requirements*, Taylor & Francis, Abingdon, England.

522 ASTM 2018. Standard Test Methods for Sampling and Testing Fly Ash or Natural Pozzolans for
523 Use in Portland-Cement Concrete. United States: American Standard Test Method. ASTM C
524 311-18.

525 ASTM 2019. Standard Specification for Coal Fly Ash and Raw or Calcined Natural Pozzolan for
526 Use in Concrete. United States: American Standard Test Method. ASTM C 618-19.

527 ASTM 2020. Standard Test Methods for Compressive Strength of Hydraulic Cement Mortars.
528 United States: American Standard Test Method. ASTM C109-20.

529 BIS 2015. Ordinary Portland Cement – Specification. New Delhi: Bureau of Indian Standards.
530 IS: 269:2015.

531 BIS 1991. Standard Sand for Testing Cement- Specification. New Delhi: Bureau of Indian
532 Standards. IS: 650:1991 (Reaffirmed 2018).

533 BSI 2019. Specification for pozzolanic materials for use with Portland cement. BSI Standards
534 Publication. BS 8615-2.

535 BIS 1967. Methods of Test for Pozzolanic Materials. New Delhi: Bureau of Indian Standards. IS:
536 1727:1967 (Reaffirmed 2018).

537 BIS 1988. Methods of Physical Tests for Hydraulic Cement-Determination of consistency of
538 standard cement paste. New Delhi: Bureau of Indian Standards.IS: 4031(Part-4):1988
539 (Reaffirmed 2019).

540 BIS 1988. Methods of Physical Tests for Hydraulic Cement-Determination of Compressive
541 Strength of Hydraulic Methods of Physical Tests for Hydraulic Cement. New Delhi: Bureau of
542 Indian Standards. IS: 4031(Part-6):1988 (Reaffirmed 2019).

543 BIS 2013. Pulverized Fuel Ash-Specification. New Delhi: Bureau of Indian Standards. IS:
544 3812:2013 (Part-1) (Reaffirmed 2017).

545 Blissett, R., Sommerville, R., Rowson, N. et al. 2017. Valorisation of rice husks using a
546 TORBED® combustion process. Fuel Processing Technology 159: 247–255, doi:
547 10.1016/j.fuproc.2017.01.046.

548 Bie, R., Song, X., Liu, Q. Ji. et al. 2018. Studies on effects of burning conditions and rice husk
549 ash (RHA) blending amount on the mechanical behavior of cement. Cement and Concrete
550 Composites 55: 162–168, doi: 10.1016/j.cemconcomp.2014.09.008.

551 Batra, V.S., Urbonaite, S., and Svensson, G. 2008. Characterization of unburned carbon in
552 bagasse fly ash. *Fuel* 87(13–14): 2972–2976, doi: 10.1016/j.fuel.2008.04.010.

553 Chen, G., Du, G., Ma, W. et al. 2015. Production of amorphous rice husk ash in a 500 kW
554 fluidized bed combustor. *Fuel* 144 :214–221, doi: 10.1016/j.fuel.2014.12.012.

555 Chandrasekhar, S., Pramada, P.N., and Majeed, J. 2006. Effect of calcination temperature and
556 heating rate on the optical properties and reactivity of rice husk ash. *Journal of Materials*
557 *Science* 41(23) : 7926–7933, doi: 10.1007/s10853-006-0859-0.

558 Chindaprasirt, P., et al. 2007. Sulfate resistance of blended cements containing fly ash and rice
559 husk ash. *Construction and Building Materials* 21(6): 1356–1361. doi:
560 10.1016/j.conbuildmat.2005.10.005.

561 Dizaji, H.B., Zeng, T., Hartmann, I. 2019. Generation of High Quality Biogenic Silica by
562 Combustion of Rice Husk and Rice Straw Combined with Pre- and Post-Treatment
563 Strategies — A Review. *Applied Sciences* 9 :1–27, doi: 10.3390/app9061083.

564 Dhandapani, Y., and Santhanam, M. 2017. Assessment of pore structure evolution in the
565 limestone calcined clay cementitious system and its implications for performance. *Cement*
566 *and Concrete Composites* 84: 36–47, doi: 10.1016/j.cemconcomp.2017.08.012.

567 Fernandes, I.J., Calheiro, D., Kieling, A.G. et al. 2016. Characterization of rice husk ash
568 produced using different biomass combustion techniques for energy. *Fuel* 165: 351–359,
569 doi: 10.1016/j.fuel.2015.10.086.

570 FAO 2018. FAO Rice Market Monitor. Food and Agriculture Organization of the United States,
571 21(1), pp. 1–38.

572 Ganesan, K., Rajagopal, K., and Thangavel, K. 2008. Rice husk ash blended cement:
573 Assessment of optimal level of replacement for strength and permeability properties of
574 concrete. *Construction and Building Materials* 22:1675–1683.

575 Gastaldini, A.L.G., Isaia, G.C., Hoppe, T.F. et al. 2009. Influence of the use of rice husk ash on
576 the electrical resistivity of concrete: A technical and economic feasibility study. *Construction*
577 *and Building Materials* 23: 3411–3419.

578 Huang, H., Gao, X., Wang, H. et al. 2017. Influence of rice husk ash on strength and
579 permeability of ultra-high performance concrete. *Construction and Building Materials*
580 149:621–628.

581 Maeda, N., Wada, I., Kawakami, M. et al. 2001. Chloride Diffusivity of Concrete Incorporating
582 Rice Husk Ash. ACI Special Publication 200: 291–308.

583 Mangat, P.S., and Ojedokun, O.O. 2018. Influence of curing on pore properties and strength of
584 alkali activated mortars. *Construction and Building Materials* 188:337–348.

585 Mali, A.K., and Nanthagopalan, P. 2021. Thermo-mechanical treatment of sugarcane bagasse
586 ash with very high LOI: A pozzolanic paradigm. *Construction and Building Materials* (in
587 press) 288 :122988, doi: 10.1016/j.conbuildmat.2021.122988.

588 Ma, H. 2014. Mercury intrusion porosimetry in concrete technology: Tips in measurement, pore
589 structure parameter acquisition and application. *Journal of Porous Materials* 21:207–215.

590 Mindess, D.S., Young, J.F., and Darwin 2003. *Concrete*, Prentice-Hall, Pearson Education, Inc.,
591 Upper Saddle River, N.J. 07458, U.S.A.

592 Nehdi, M., Duquette, J., and El Damatty, A. 2003. Performance of rice husk ash produced using
593 a new technology as a mineral admixture in concrete. *Cement and Concrete Research* 33(8)
594 : 1203–1210, doi: 10.1016/S0008-8846(03)00038-3.

595 Nair, D.G., Jagadish, K.S., and Fraaij, A. 2006. Reactive pozzolanas from rice husk ash: An
596 alternative to cement for rural housing. *Cement and Concrete Research* 36(6): 1062–1071,
597 doi: 10.1016/j.cemconres.2006.03.012.

598 Olalekan, O., and Mangat, P.S. 2018. Characterization and Pore Structure of Rice Husk Ash
599 Cementitious Materials. ACI Special Publication: Durability and sustainability of concrete
600 structures 326: 8.1-8.10.

601 Rozainee, M., Ngo, S.P., Salema, A.A. et al. 2008. Fluidized bed combustion of rice husk to
602 produce amorphous siliceous ash. *Energy for Sustainable Development* 12(1): 33–42, doi:
603 10.1016/S0973-0826(08)60417-2.

604 Rêgo, J.H.S., Nepomuceno, A.A., Figueiredo, E.P. et al. 2015a. Microstructure of cement
605 pastes with residual rice husk ash of low amorphous silica content. *Construction and*
606 *Building Materials* 80:56–68, doi: 10.1016/j.conbuildmat.2014.12.059.

607 Rêgo, J.H.S. et al. 2015b. Effect of Particle Size of Residual Rice-Husk Ash in Consumption of
608 $\text{Ca}(\text{OH})_2$. *Journal of Materials in Civil Engineering* 27(6): 04014178, doi:
609 10.1061/(asce)mt.1943-5533.0001136.

- 610 Singh, B. 2018. Rice husk ash. Waste and Supplementary Cementitious Materials in Concrete:
611 Characterisation, Properties and Applications, Elsevier. pp. 417-460, doi: 10.1016/B978-0-
612 08-102156-9.00013-4.
- 613 Singh, A., and Singh, B. 2020. Characterization of rice husk ash obtained from an industrial
614 source. *Journal of Sustainable Cement-Based Materials* 10(4): 193-212, doi:
615 10.1080/21650373.2020.1789010.
- 616 Van, V.T.A., Rößler, C., Bui. D.D. et al. 2013. Mesoporous structure and pozzolanic reactivity of
617 rice husk ash in cementitious system. *Construction and Building Materials* 43: 208–216, doi:
618 10.1016/j.conbuildmat.2013.02.004.
- 619 Venkatanarayanan, H.K., and Rangaraju, P.R. 2013. Material Characterization Studies on Low-
620 and High-Carbon Rice Husk Ash and Their Performance in Portland Cement Mixtures.
621 *Advances in Civil Engineering Materials* 2 : 20120056.
- 622 Wada, I., Kawano, T., Kawakami, M. et al. 2000. Effect of Highly Reactive Rice Husk Ash on
623 Durability of Concrete and Mortar. *ACI Special Publication* 192:205–222.
- 624 Xu, W., Lo, T.Y., and Memon, S.A. 2012. Microstructure and reactivity of rich husk ash.
625 *Construction and Building Materials* 29: 541–547, doi: 10.1016/j.conbuildmat.2011.11.005.
- 626 Zunino, F., and Lopez, M. 2017. A methodology for assessing the chemical and physical
627 potential of industrially sourced rice husk ash on strength development and early-age
628 hydration of cement paste. *Construction and Building Materials* 149: 869–881, doi:
629 10.1016/j.conbuildmat.2017.05.187.
- 630 Zain, M.F.M., Islam, M.N., Mahmud, F. et al. 2011. Production of rice husk ash for use in
631 concrete as a supplementary cementitious material. *Construction and Building Materials*
632 25(2) : 798–805, doi: 10.1016/j.conbuildmat.2010.07.003.

633

634 **List of Figure Legends:**

635 Figure 1. SEM images of the all RHAs (1000x) (a) R1 (b) R2 (c) R3 (d) R4 (e) R5 (f) R6 g) R5-
636 G100 (2000x) and h) R6-G100 (2000x).

637 Figure 2. Cement replacement versus a) Consistency of control and beneficiated RHA, R5
638 blended pastes b) Water-binder ratio of mortars associated with consistency of pastes.

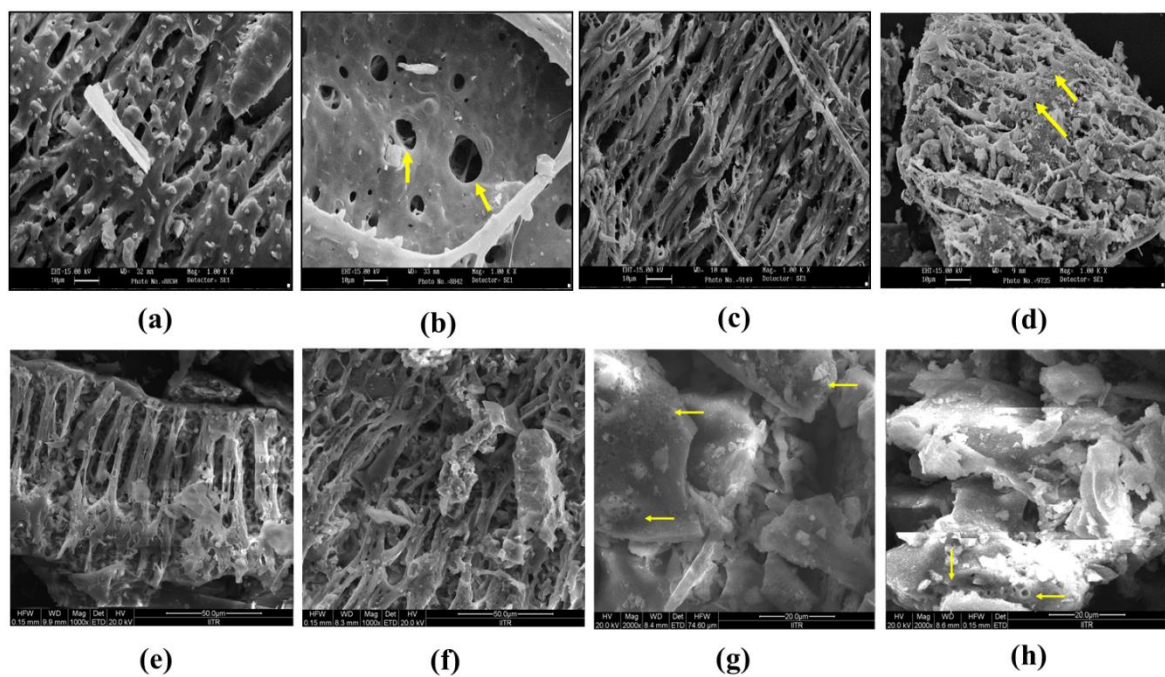
639

640 Figure 3. Compressive strength versus cement replacement for the control and beneficiated
641 RHA blended mortars as per IS 4031 (Part 6) (BIS, 1988) at (a) 7-day (b) 28-day and (c) as per
642 ASTM C 109 (ASTM, 2020) at 7- and 28-day.

643 Figure 4. a) Cumulative Pore volume distribution of the PC and RHA blended mortars, and b)
644 Relationship between pore volume and incremental pore diameter range.

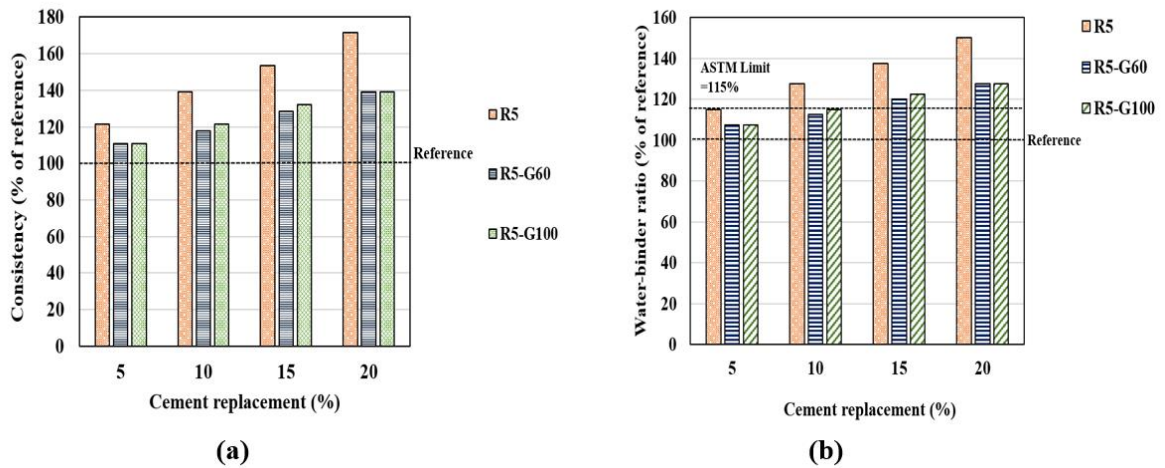
645

646



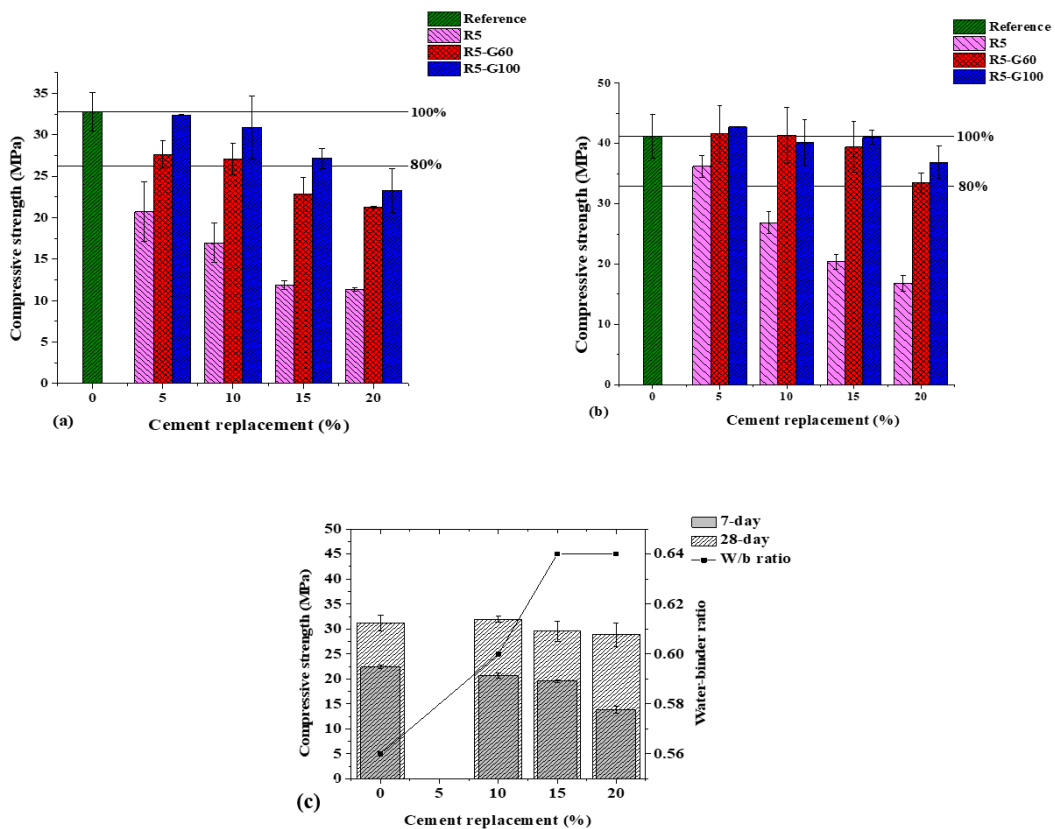
647

648 **Figure 1: SEM images of the all RHAs (1000x) (a) R1 (b) R2 (c) R3 (d) R4 (e) R5 (f) R6 g)**
649 **R5-G100 (2000x) and h) R6-G100 (2000x).**



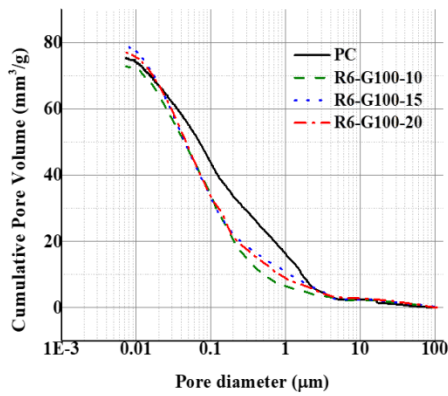
650
651
652
653
654

Figure 2: Cement replacement versus a) Consistency of control and beneficiated RHA, R5 blended pastes b) Water-binder ratio of mortars associated with consistency of pastes.

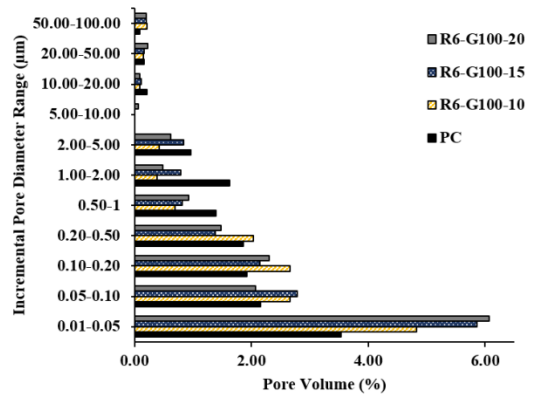


655
656
657
658
659

Figure 3: Compressive strength versus cement replacement for the control and beneficiated RHA blended mortars as per IS 4031 (Part 6) (BIS, 1988) at (a) 7-day (b) 28-day and (c) as per ASTM C 109 (ASTM, 2020) at 7- and 28-day.



(a)



(b)

660

661 **Figure 4: a) Cumulative Pore volume distribution of the PC and RHA blended mortars,**

662 **and b) Relationship between pore volume and incremental pore diameter range.**

663

664

665

666

667

668

669

670

671

672

673

674

675

676

677

678

Table 1. Properties of the as-received, control and beneficiated RHA samples.

	R1	R2	R3	R4	R5	R6	R5-G60	R5-G100	R6-G100
Chemical composition (%)									
Na ₂ O	0.11	0.13	0.75	0.29	0.83	0.49	-	-	-
MgO	0.28	0.33	0.56	0.64	0.90	0.71	-	-	-
Al ₂ O ₃	0.10	0.11	0.59	2.57	2.28	1.58	-	-	-
SiO ₂	61.3	70	80	72.2	80.2	84.4	-	-	-
P ₂ O ₅	1.1	1.24	0.83	0.62	0.65	0.46	-	-	-
SO ₃	0.45	0.52	0.66	0.21	0.31	0.15	-	-	-
K ₂ O	2.2	2.56	1.60	6.12	4.07	3.07	-	-	-
CaO	0.49	0.55	0.97	1.26	1.16	0.63	-	-	-
TiO ₂	-	-	-	-	0.09	0.08	-	-	-
MnO	0.15	0.17	0.08	0.07	0.15	-	-	-	-
Fe ₂ O ₃	0.4	0.45	0.41	1.49	1.1	0.71	-	-	-
Cl	0.32	0.37	0.55	0.98	0.42	0.35	-	-	-
LOI* (%)	33	23.4	13	14	7.7	7.3	-	-	-
Amorphous SiO ₂ (%)	61.3	70	75	64	70	80	-	-	-
Total Amorphous (%)	100	100	95	92	90	95	-	-	-
Wet Sieve Analysis									
(% passing)									
75 µm	11	25	20.4	10	12.1	10.5	77.9	82.9	83.08
45 µm	8.5	20	8.9	2.5	7.4	7.2	66.6	70.4	71.4
BET-SSA (m²/g)	49	42	32	15	26	32	32	35	43
Specific Gravity	1.63	1.7	1.8	1.9	2.15	2.10	2.19	2.2	2.16
Average Particle Size, d₅₀ (µm)	-	-	-	-	171	228	22	18	25
Pozzolanic reactivity (%)									
7-day	43.81	57.78	69.72	67.19	76.70	73.81	86.40	93.60	99.97
28-day	52.33	62.81	79.21	75.10	84.50	85.98	94.70	96.20	97.88
Water requirement (% of reference)	120	118	114	114	113	113	109	107	107

*LOI: Loss On Ignition

Table 2: Pore system parameters for the PC and RHA blended mortars.

Mix	Porosity		Pore Diameters (μm)			Pore Volumes (%)		
	Intrudable (mm^3/g)	Porosity (%)	Threshold (d_{th})	Critical (d_c)	Average (d_{avg})	Pore Diameter Range (μm)		
						<0.01	0.01 - 0.05	>0.05
PC	75.42	13.92	3.012	0.0898	0.057	0.27	3.47	10.18
R6-G100-10	72.80	14.30	2.000	0.1000	0.048	0.15	4.83	9.32
R6-G100-15	79.34	15.11	3.009	0.0311	0.042	0.36	5.72	9.03
R6-G100-20	76.99	14.55	2.003	0.1593/ 0.0480	0.046	0.25	5.19	9.11

Supplementary material

Table S1: Identification of the RHA samples.

No.	Sample	Nomenclature	Source	Combustion Technique	Combustion Temperature	Region	Grinding Time (mins.)
1	As-received	R1	Gosai Rice Mills, Bijabahal, Odisha.	Unknown	Unknown	East	-
2		R2	Jai Bhawani Agencies, Gulbarga, Karnataka.	Unknown	Unknown	South	-
3		R3	Hari Om Traders, Junagadh, Gujrat.	Unknown	Unknown	West	-
4		R4	Kwantum Papers, Hoshiarpur, Punjab.	Fluidised Bed	Unknown	North	-
5	Control	R5	Kwantum Papers, Hoshiarpur, Punjab.	Fluidised Bed	600°C-700°C	North	-
6		R6	Kwantum Papers, Hoshiarpur, Punjab.	Fluidised Bed	650°C -700°C	North	-
7	Beneficiated	R5-G60					60
8		R5-G100	-do-	-do-			100
9		R6-G100					100

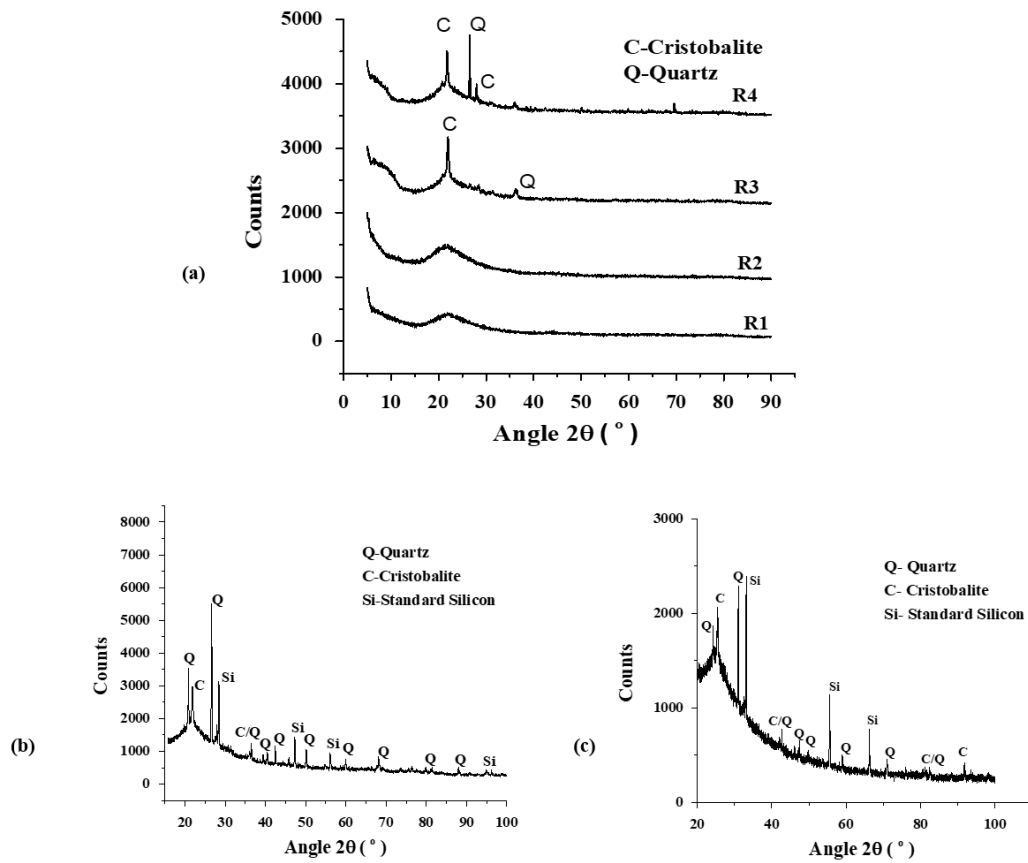


Figure S1: X-ray diffractogram of (a) R1, R2, R3, R4 (b) R5 and (c) R6.

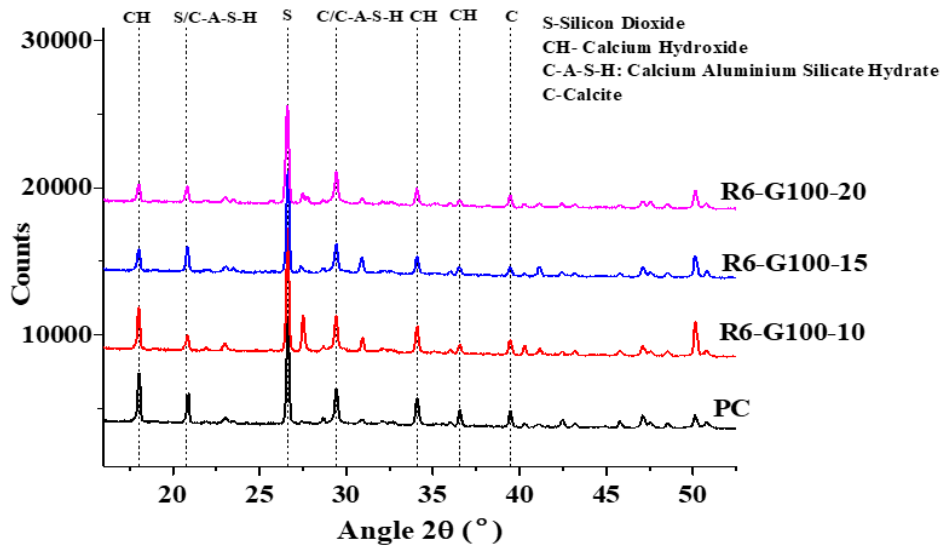


Figure S2: XRD patterns for the PC and the blended mortars after curing for 28-days.

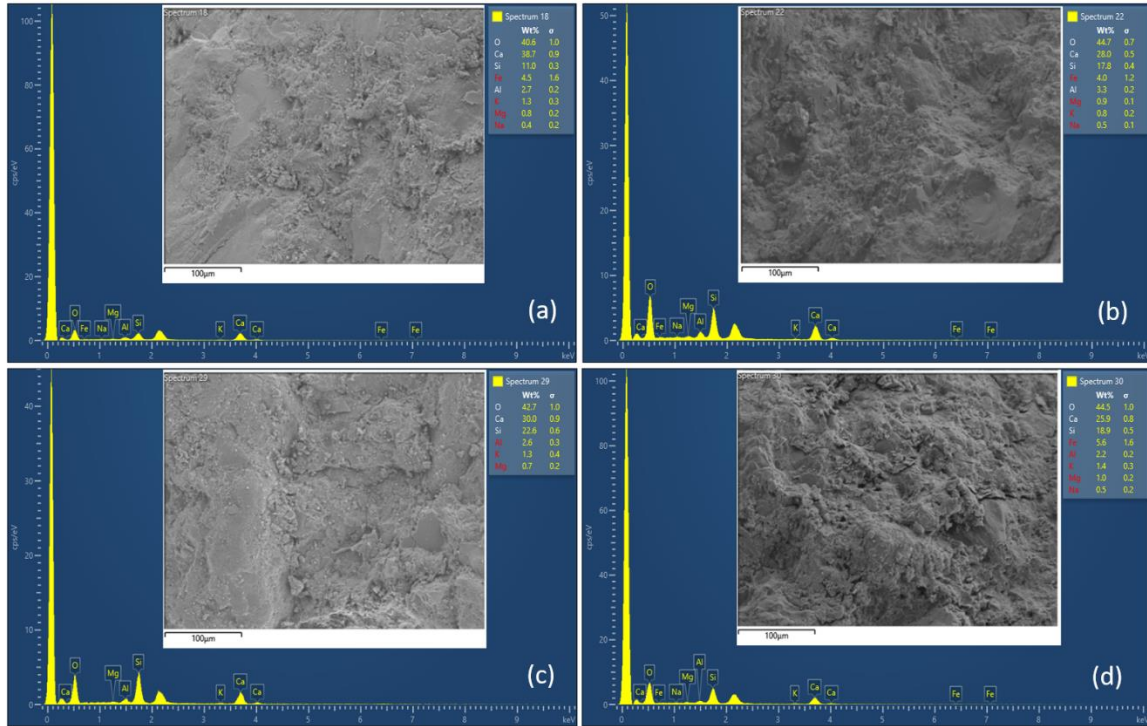


Figure S3: SEM and EDX of mortars at 28-days a) PC b) R6-G100-10 c) R6-G100-15 and d) R6-G100-20

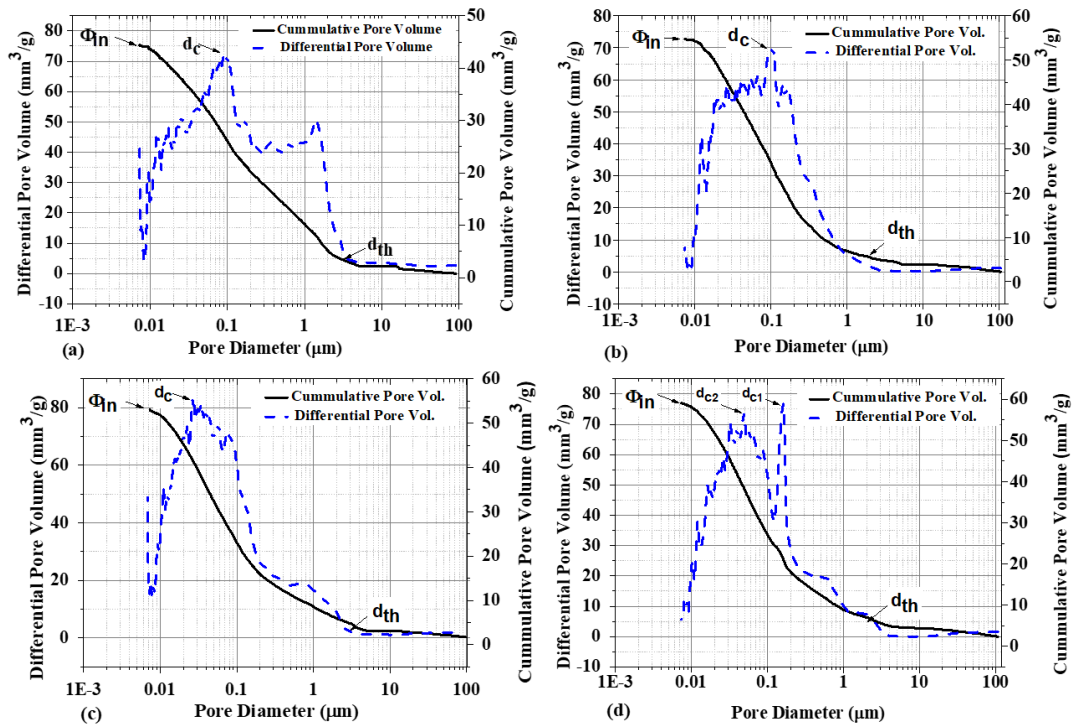


Figure S4: Pore size distribution for mortars a) PC b) R6-G100-10 c) R6-G100-15 and d) R6-G100-20